# Conformational fluxionality of long-chain alkene clusters in the gas phase evidenced from a combined experimental and theoretical approach

Caroline Smith Lewin, O. Herbinet, P. Arnoux, F. Battin-Leclerc, G A Garcia, L. Nahon, L S Tran, G. Vanhove, M. Mogren Al Mogren, M. Hochlaf, et al.

# Conformational Fluxionality of Long-Chain Alkene Clusters in the Gas Phase Evidenced from a Combined Experimental and Theoretical Approach

C. Smith Lewin,[a] O. Herbinet,[a] P. Arnoux,[a] F. Battin-Leclerc,[a] G. A. Garcia,[b] L. Nahon,[b] L. S. Tran,[c] G. Vanhove,[c] M. Mogren Al Mogren,[d] M. Hochlaf,[e] F. Calvo[e], and J. Bourgalais[a,1]

[1]*Université de Lorraine, CNRS, LRGP, F-54000 Nancy, France.*

[2]*Synchrotron SOLEIL, L'Orme des merisiers, Départementale 128, 91190 Saint-Aubin, France*

[3]*Université Lille, CNRS, PC2A, F-59000 Lille, France*

[4]*Department of Chemistry, College of Sciences, King Saud University, P.O. Box 2455, Riyadh 11451, Saudi Arabia*

[5]*Université Gustave Eiffel, COSYS/IMSE, 5 Bd Descartes, 77454, Champs sur Marne, France*

[6]*Université Grenoble Alpes, CNRS, LiPhy, Grenoble 38000, France*

ABSTRACT

Clusters bound by weak, non-covalent forces such as van der Waals interactions and hydrogen bonds are ubiquitous in dilute media ranging from aerosols to molecular fluids and biological structures, their interest being fundamental as in astrochemistry, but also more applied as in organic electronics. Neutral clusters of up to six 1-hexene molecules produced by supersonic expansion of a gas mixture were ionized, mass selected, and spectroscopically characterized using synchrotron-based VUV photoelectron photoion coincidence (PEPICO) technique. Ionization energies inferred from these measurements show decreasing trends as the cluster size increases, by about 0.5 eV over the range of 1-6 molecules. Dedicated theoretical DFT-based calculations were performed to unravel the possible structures of these clusters and determine their vertical and adiabatic ionization energies. Our computational search for stable structures considered the possible chirality effects associated with most conformers of the monomer having enantiomers, in an approach with a broad structural sampling employing classical force fields followed by systematic re-optimization using an efficient quantum chemical method. Vertical and adiabatic ionization energies obtained using wavefunction-based methods exhibit significant dispersion due to conformational flexibility already in the monomer, but these effects are magnified in clusters due to their fluxionality at the experimental temperature of about 130 K. Overall, the trends obtained for the calculated vertical ionization energies agree well with the measured data, and suggest that possible chiral recognition effects that could stabilize specific structures are likely to be hampered at the experimental temperature.

[1] Corresponding author: jeremy.bourgalais@cnrs.fr
Currently at: Université de Rennes, CNRS, IPR, F-35000 Rennes, France.

## I. INTRODUCTION

Weak intermolecular forces play a pivotal role in many areas of physical, chemical, and biological phenomena encompassing notably solvation, nucleation and aerosol formation [1],[2]. Consequently, extensive experimental and theoretical investigations have been undertaken to deepen our understanding of such interactions, at the molecular and macroscopic scales alike. Over time, experimental research has evolved to consider not only bulk materials whose behavior is ruled by macroscopic thermodynamics and kinetics, but also atomic and molecular clusters in the gas phase, serving as a crucial bridge between the gaseous and condensed phases [3]–[11]. Experimental measurements can be performed on size-selected compounds and often as time-resolved processes, providing key insight into the diverse mechanisms of cluster formation and relaxation that are typically marked with strong and irregular variations with size. However, and despite the importance of these weakly bound complexes, comprehensive data on their structures and electronic properties often remain difficult to access, precisely owing to the strong dependence of their structural and dynamical features on their size. Even simple clusters can exist in numerous isomeric forms, with the predominant structure influenced by factors such as the presence of a dopant or impurities as well as external factors such as temperature or pressure. Methane ($CH_4$) serves as an exemplary organic compound whose cluster properties significantly depend on the cluster size. In methane clusters, multiple molecules associate through non-covalent interactions, leading to distinct physical and chemical properties based on the number of molecules involved [12],[13].

Studies of weakly bound systems employ a range of spectroscopic techniques to reveal structural and electronic properties. Infrared (IR) and microwave (MW) spectroscopy provide rather direct structural insights by probing vibrational and rotational modes, essential for understanding intermolecular interactions and cluster geometry [6],[14]. Photoionization (PI), widely recognized as a universal probe, enables tracking of electronic changes across diverse systems. Techniques like high-harmonic generation (HHG) can monitor atomic cluster expansion with high temporal resolution [15] and probe electron scattering, as was achieved for water clusters [16]. Photoelectron spectroscopy (PES) is also a powerful technique for studying the electronic and structural properties of weakly bound systems, particularly clusters. Angle-resolved PES provides additional structural insights by revealing anisotropy values across size distributions [17],[18]. Advances in synchrotron radiation light sources have elevated the capabilities of PES through their energy tunability, narrow-band emission, and high brilliance [19]. These characteristics support more sophisticated coincidence measurements and techniques such as mass-selected threshold photoelectron spectra (ms-TPES) through synchrotron-based VUV photoelectron photoion coincidence (SVUV-PEPICO) [20],[21].

However, and as is the case with other spectroscopic techniques, the successful interpretation of experimental signals in PEPICO measurements requires the support of dedicated quantum calculations. Theory is particularly essential in neutral van

der Waals clusters, for which the dramatic nature of ionization makes them particularly prone to Jahn-Teller (JT) distortion [22]. In turn, JT effects could make the ground state vibrational level of the ion to be located outside of the Franck-Condon (FC) region that would be accessed by direct photoionization of the corresponding neutral system, affecting the spectroscopic transitions and complicating their interpretation. Van der Waals molecular clusters are also characterized by marked differences between intra- and intermolecular forces, which give rise to many low-energy minima in their energy landscapes, competing with each other but separated by large amplitude rearrangements. Clusters made from polycyclic aromatic hydrocarbons (PAH), for example, exhibit various stacking geometries that subtly depend on the details of the interactions, including quadrupolar forces [23]. In such systems, the presence of numerous relatively low energy barriers between different configurations makes them responsive to even minor shifts in electronic state energies induced by the JT effect. Additionally, the coupling of electronic states with vibrational modes, especially those involving loose motions like intermonomer bending or concerted stretching of intermolecular bonds modes, can result in notable changes in geometry. Only a sufficiently accurate quantum mechanical approach can correctly capture these effects and describe the energetic and structural evolution of non-covalent molecular clusters upon ionization [24].

In recent years, part of the experiments conducted at synchrotron facilities combined with dedicated computational modeling focused on molecular clusters formed from hydrocarbon molecules, including PAHs [25], small clusters like methane [12], and small non-organic molecular species such as water [26],[27]. The interest in PAHs lies into their clustering through van der Waals forces, which is thought playing a key role in soot formation during combustion [28]–[31], especially in dimer formation [32]–[37]. Additionally, PAHs are ubiquitous in the astrochemical contexts [38],[39], where their formation mechanisms and possible clustering have been an active subject of research due to their implication for interstellar infrared emission bands, the formation of larger carbon structures, ices, and complex organic molecules [40]–[47]. In contrast, limited attention has been paid to the arrangement and electronic properties of clusters made of linear olefins with long carbon chains, despite their potential to drive innovation across multiple sectors such as energy, environmental sustainability, and materials engineering [48].

In the present work, experimental photoelectron spectra of gas-phase 1-hexene ($C_6H_{12}$, m/z 84) small neutral clusters are reported for the first time, as measured from VUV photoelectron photoion coincidence (PEPICO) spectroscopy. Interpretation of the measurements was carried out using multi-approach atomistic modeling, encompassing exhaustive sampling based on force fields, systematic refinement using explicit electronic structure methods, and wavefunction-based determination of the vertical (VIE) and adiabatic (AIE) ionization energies. Our modeling notably accounts for the numerous possible conformers of the monomers, which leads to an appreciable combination when forming clusters owing to the presence of enantiomers. The conformational diversity arising from our exploration appears to be particularly significant, especially at the estimated

experimental temperature in excess of 130 K, as determined in previous studies using a similar setup [26],[49]. This combined experimental and theoretical study reveals a pronounced decrease in size effects, primarily attributed to the presence of stabilizing non-covalent interactions. Structural effects are important not only on the diversity of the underlying neutral clusters, but also, unsurprisingly, on the predicted ionization energies.

## II. EXPERIMENTAL SETUP

1-hexene clusters were produced using a continuous supersonic expansion of a gas mixture made of helium with 0.5% of 1-hexene. The liquid fuel was uniformly mixed with the carrier gas flow and evaporated through a controlled evaporator mixer upstream of a 70 μm pinhole, allowing adiabatic expansion of the resulting vapor into the SAPHIRS primary vacuum chamber located on the VUV DESIRS undulator-based beamline at the SOLEIL synchrotron in Saint-Aubin, France [50]. The backing pressure of He was adjusted to maximize the production of 1-hexene clusters. The beam of 1-hexene clusters was skimmed twice before entering the DELICIOUS III $i^2$PEPICO spectrometer and crossing at a right angle a monochromatized beam of VUV photons [51],[52]. Photoelectrons and photoions, accelerated in opposite directions by a static electric field, were subsequently detected in coincidence on two dedicated imaging detectors using a modified Wiley−McLaren imaging time-of-flight spectrometer on the ion side and a photoelectron VMI spectrometer on the electron side. However, in this work, the ion imaging functionality of the setup was not utilized. DELICIOUS III allows the acquisition of TPES by integrating the near-zero kinetic energy (< 50 meV) electron signal at each photon energy [53]–[55]. For the measurement of TPES, the photon energy was scanned in steps of 10 meV from 8 eV up to 10.5 eV, covering the range of ionization energies of hexene monomer and small-sized hexene clusters. At each photon energy, the coincident electron and ion signals were recorded for up to 50 s. The mass spectrum displayed in FIG. 1 shows the relative intensity distribution of the 1-hexene clusters obtained under these experimental conditions. The carrier gas's backup pressure was adjusted to optimize cluster production, as observed with a maximum size of $m/z$ = 504, corresponding to the hexamer.

Note that only mass selection was achieved here, not genuine mass selection, because dissociative photoionization contributions cannot easily be ruled out [25],[56]–[58], as indicated by the increased peak width as a function of cluster size (see FIG. 1). The excess energy in the cationic cluster increases until fragmentation, predominantly through the loss of a

monomer unit: $M_n^+ \rightarrow M_{n-1}^+ + M$ [25],[59]. However, the fragmentation energy of clusters formed by 1-hexene monomers could plausibly exceed their ionization energy significantly, despite the lack of π-conjugation typically associated with enhanced stability in molecules like PAHs. In 1-hexene clusters, the stabilization primarily arises from van der Waals forces, which, although weaker and non-directional compared to hydrogen bonds, allow for structural flexibility and efficient redistribution of excess energy upon ionization. This internal energy dissipation through vibrational modes spreads the energy more evenly, reducing the risk of immediate localized bond breakage and potentially raising the fragmentation threshold. Furthermore, the intermolecular interactions within the cluster can collectively stabilize the system, with the cluster environment possibly offering additional resistance to fragmentation compared to isolated monomers. This hypothesis is supported by appearance energy calculations for the clusters, based on the energies of the neutral and ionized structures presented later in this work. Assuming barrierless reactions due to weak interactions like in the pyrene dimer [25], the appearance energies are estimated to lie 0.4–0.5 eV above their adiabatic ionization energies. Consequently, no contamination from potential fragmentation processes is expected to affect the adiabatic values reported here. However, this may not necessarily hold true for the vertical values.

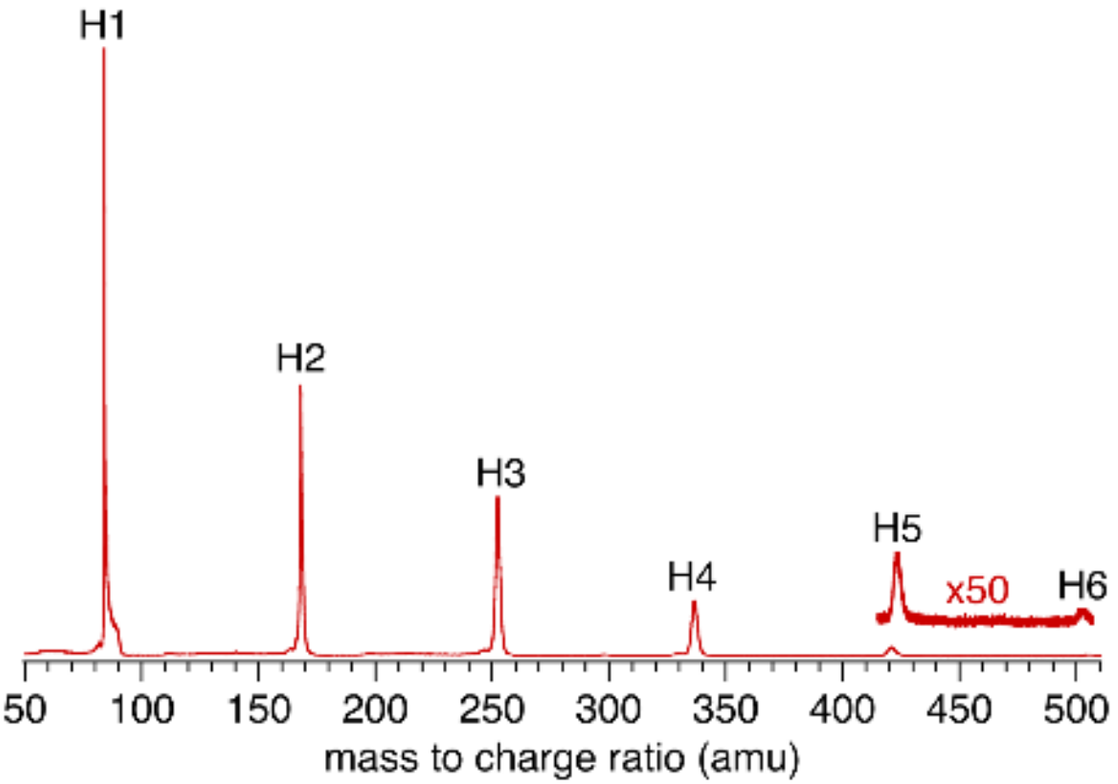


FIG. 1. Mass spectrum showing the 1-hexene cluster distribution from the time-of-flight spectrometer recorded at the photon energy of 10.5 eV. The label H*n* with *n*=1-6 refers to the number of monomer units within the clusters.

## III. THEORETICAL METHODS

Interactions in neutral clusters made from 1-hexene decouple the intramolecular, covalent forces inherent to individual hexene monomers from intermolecular, non-covalent forces that are of much lower magnitude. Those forces affect the various degrees of freedom very differently, conformers of 1-hexene being tied to hydrocarbon chemistry that constrains most internal coordinates of bond lengths, bending and torsion angles according to the hybridization level of each carbon atom, while non-covalent interactions are responsible for the relative orientations of molecules within the clusters. The balance between inter- and intramolecular interactions, as well as external parameters such as temperature, eventually dictate which conformers are present in the cluster and how the various monomers are (weakly) bound to each other.

The 1-hexene monomer supports 14 different three-dimensional conformers that differ upon 120° rotations around $sp^3$ C-C bonds, only conformer D being achiral and with a planar carbon backbone. FIG. 2 shows their corresponding stable geometries obtained from density-functional theory (DFT) calculations performed using the wB97xD functional and the 6-

311++G** basis set. This range-corrected hybrid density functional was chosen owing to its known good performance for molecular clusters [60],[61] and in particular its essential inclusion of non-covalent interactions. In FIG. 2, these monomers are labelled A–N and ordered by decreasing relative stability, A being the most stable form.

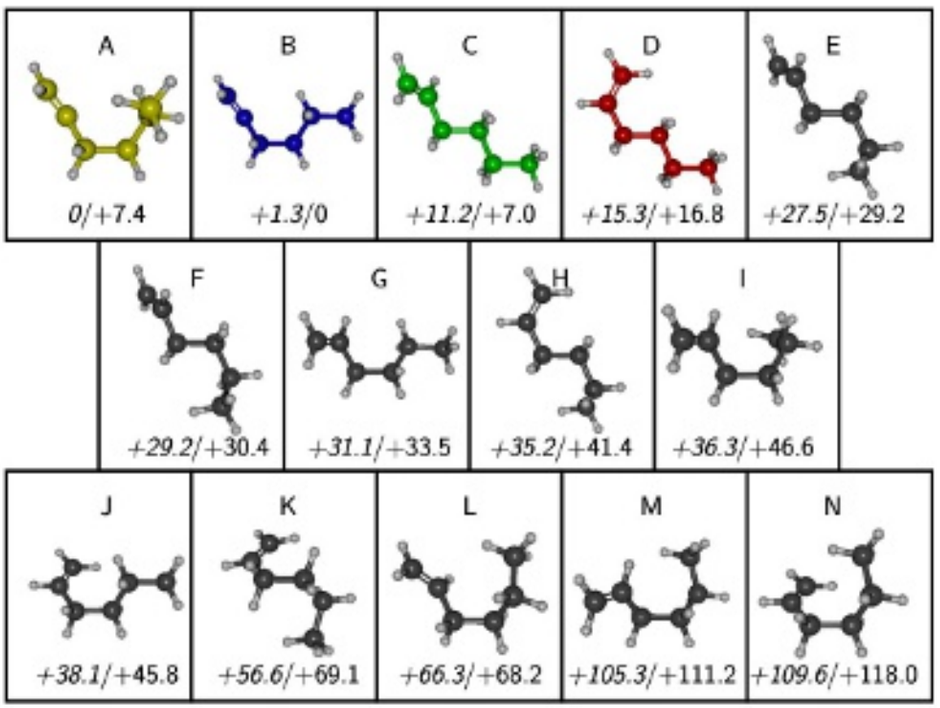


FIG. 2. Conformers of 1-hexene computed at the DFT/wB97xD/6-311++G** level of theory, labelled as A-N by increasing energy with this method, the relative energies (meV) being given *without*/with the harmonic zero-point energy correction. The most stable conformers A-D used to generate the larger size clusters are highlighted in colors.

Under the low temperature experimental conditions, intramolecular fluxionality can be hindered, while intermolecular degrees of freedom remain relatively soft and accessible. In the purpose of efficiently generating candidate structures for clusters, we assume that they combine the 27 available conformers, including 13 pairs of enantiomers that we denote as X/X* for all X in the A-N series, except for X=D that is the achiral conformer with a planar carbon backbone. Treating the conformers as rigid, classical force fields accounting for long-range van der Waals and multipolar electrostatics can be employed to model the intermolecular interactions, and here we resort to the simple Amber *ff99* model [62], which further enables fast screening of putative global minima using standard optimization methods. The individual charge distributions on each monomer were obtained using the same DFT method and the ESP electrostatic potential fitting procedure [63]. They are provided as

supplementary electronic material for the 14 monomers A-N. In the present work we have considered parallel tempering Monte-Carlo combined with systematic quenches, for large series of combinations between prescribed conformers, ignoring combinations if their global enantiomeric counterpart had already been considered (X/Y* versus X*/Y). Successive optimizations of the lowest-energy conformers at the DFT level revealed that only combinations of specific conformers contributed to the putative global minima of cluster. In practice, all (196) possible combinations were considered for the dimers, resulting in A-E combinations being significantly lower. For trimers and larger clusters, the search was sequentially restricted to combinations of A-E (trimers), A-D (tetramers), B-D (pentamers), and C-D (hexamers to octamers).

All parallel tempering simulations employed a series of 32 temperatures distributed geometrically in the 5 – 500 K temperature range and $10^7$ Monte Carlo cycles for each temperature. Following this large-scale screening at the level of force field, the most stable clusters obtained at all monomer compositions were further reoptimized at the DFT level using again the wB97xD/6-311++G** method. For each cluster size, the most stable structure obtained at the DFT level was taken as the putative global minimum. Occasionally, the inclusion of zero-point energy in the harmonic approximation produced alternative lowest-energy isomers, in which case these two competing structures were both considered for further scrutiny in the cationic state.

To interpret PEPICO measurements, vertical and adiabatic ionization energies were first computed using the same DFT approach already employed to refine the geometries of the neutral clusters, correcting adiabatic values for the contribution of zero-point motion in the harmonic approximation. Unfortunately, while DFT is reliable for geometries it is more disputable for absolute energies [52]–[55] and we also considered alternative quantum chemical methods to determine ionization energies. Post Hartree-Fock computations were performed at the (R)MP2, (R)MP2-F12 and (R)CCSD(T) levels of theory, as implemented in MOLPRO 2015 [68]. For vertical ionization energies (VIEs), such computations consist of single point calculations for monomers and small 1-hexene clusters at their DFT optimized geometries, both the neutrals and the cations being reoptimized at the respective post Hartree-Fock levels for the adiabatic ionization energies (AIEs) evaluations. Here, the atoms were described using the aug-cc-pVDZ basis set [69],[70] with the corresponding density fitting functions as generated by MOLPRO.

## IV. RESULTS AND DISCUSSION

### A. Hexene monomer

The fourteen topologically distinct conformers of 1-hexene, illustrated in FIG. 1, are in themselves a potential major cause of fluctuations in the experimental observables and calculated properties already for the monomer. In FIG. 3, these conformers have been ranked as a function of increasing DFT energy, including the zero-point correction in the harmonic approximation. This figure also shows the cumulated thermal probability of these conformers at the experimentally estimated temperature of 130 K, evaluated as Boltzmann weights in the same harmonic approximation.

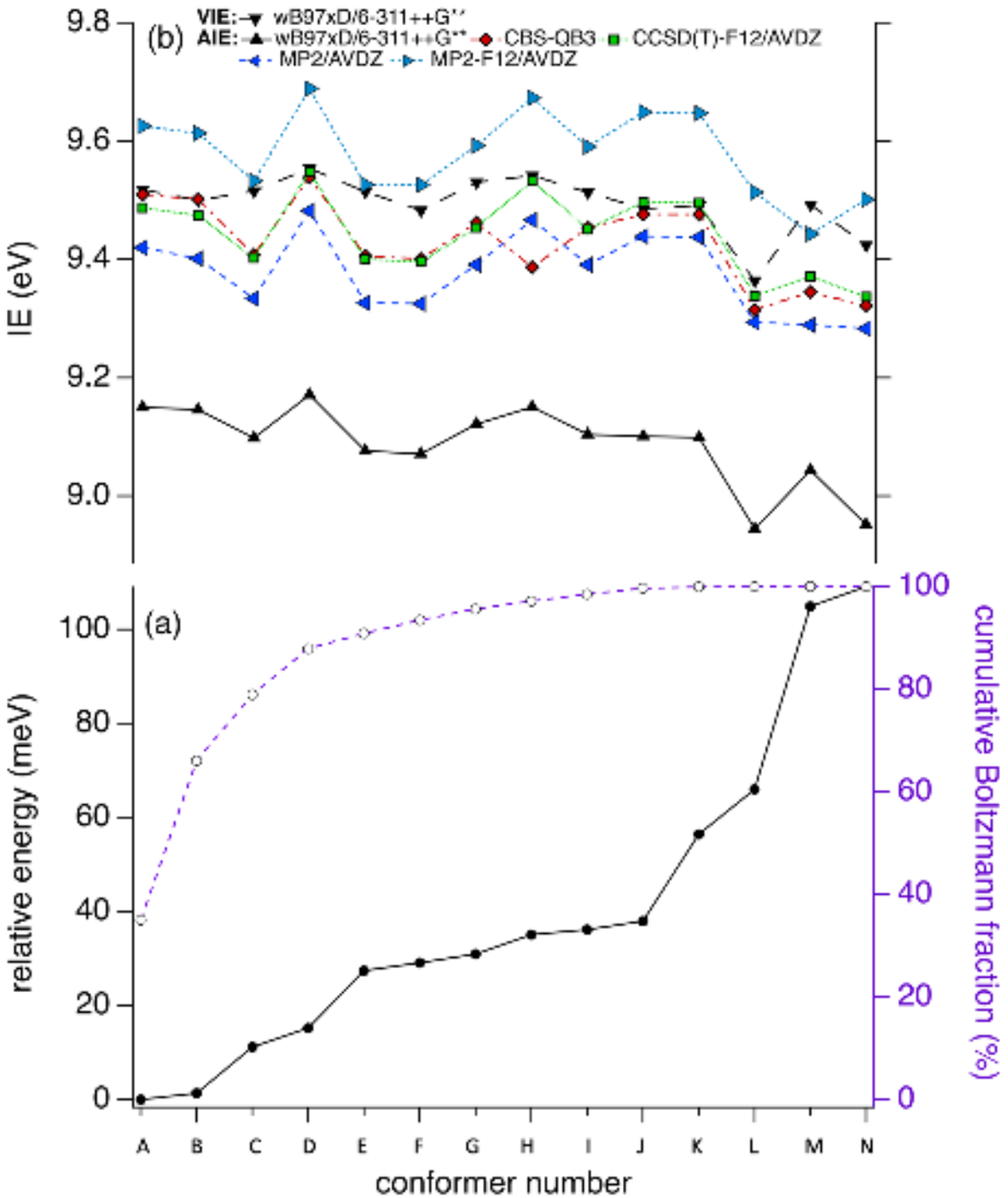


FIG. 3. (A) Relative energy (black dots) between monomer conformers obtained at the DFT/wB97xD/6-311++G** level of theory and cumulative Boltzmann fraction at 130 K (open purple dots); (B) Vertical ionization energy (VIE) predicted from DFT/wB97xD/6-311++G** (black downward triangles) and adiabatic ionization energy (AIE) predicted from different quantum chemical methods: DFT/wB97xD/6-311++G** (black triangles), CBS-QB3 (red diamonds), CCSD(T)-F12/aug-cc-pVDZ (green squares), MP2/aug-cc-pVDZ (blue upward triangles), and MP2-F12/aug-cc-pVDZ (blue dashed upward triangles). Note that all the numerical data from FIG. 3 are also provided in Table S1.

As shown by this figure, about 88% of 1-hexene should be in any of first four lower energy conformers at thermal equilibrium. The ionization energies associated with all conformers were determined using various quantum chemical methods, starting with the same DFT approach used to optimize the structures and energies in FIGs. 2 and 3, respectively. From

DFT/wB97xD/6-311++G** we have thus determined the vertical and adiabatic values, which are also reported in the upper panel of FIG. 3. Using this method, AIE values lie in the range 8.94-9.17 eV depending on the conformer, vertical values showing values that are markedly higher by about 0.3–0.4 eV, and also slightly narrower fluctuations of 0.19 eV [see FIG. S1 for the entire distributions of AIE and VIE values]. Wavefunction-based approaches were also employed for comparison, namely MP2, MP2-F12 and CCSD(T)-F12, all using the aug-cc-pvDZ basis set, providing single point energies in both the neutral and the cationic structures determined by DFT. These alternative calculations lead to AIE values that are substantially higher by 0.3–0.4 eV [see FIG. S2], also superimposed in FIG. 3. Wavefunction-based methods yield systematically higher AIE values because they rigorously capture electron correlation, avoid delocalization errors, and fully incorporate HF exchange, particularly in the ionized states where these effects are pronounced [71]. In addition, we also determined the adiabatic ionization energies using the CBS-QB3 method [72],[73], the results of which are also given in FIG. 3. The CBS-QB3 approach combines a DFT optimization step with single-point energies for both the neutral and cationic states corrected at the CCSD(T) level of theory, plus an extrapolation to the complete basis set limit. Considering the similarity of this approach with our own DFT/CCSD(T)-F12 composite scheme, it is not surprising that the resulting AIE agree well with these values, the main discrepancy of about 0.2 eV being found for conformer H.

Temperature effects on the ionization energies can be roughly evaluated using again the harmonic approximation for the canonical weights, the resulting AIE being found about 30 meV lower than the zero-temperature value of the lowest-energy structure [see FIG. S3]. This sets a lower limit that we can expect on intrinsic accuracies of the calculated ionization energies.

FIG. 4 shows the experimentally measured TPES of m/z 84, corresponding to the 1-hexene monomer. To simulate transitions between vibrational levels of the lowest-energy neutral conformers and their cations, the time-independent adiabatic Hessian Franck-Condon (TI-AH|FC) model was used within the harmonic approximation [74]. Temperature effects were again considered at 130 K, the resulting stick spectrum was then convolved using Gaussian functions with half-widths at half-maximum (HWHM) of 200 $cm^{-1}$ to match the experimental resolution. As carried out before [75], the 0–0 transition of the computed stick spectra was adjusted to match the experimental spectra within the uncertainty of the energy calculation. The FC factors thus calculated for the lowest-energy conformers A–D are superimposed in FIG. 4 as a function of increasing binding energy. The FC factors determined for the remaining conformers of 1-hexene are given as supplementary material [see FIG. S4].

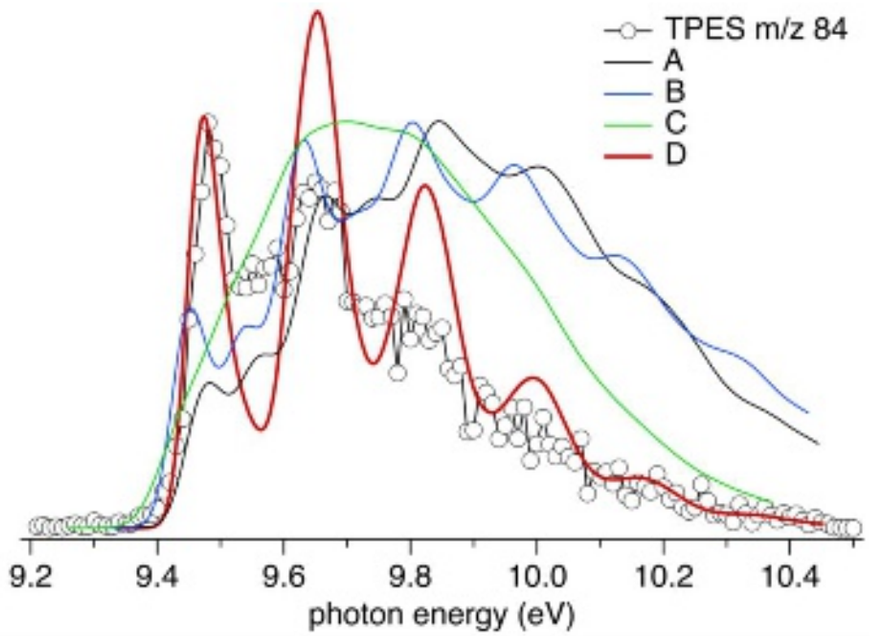


FIG. 4. Experimental TPES of m/z 84 (open dots) and simulated PES determined from the FC factors calculated for the lowest-energy conformers A–D of 1-hexene.

The simulated spectra of these low-lying conformers align well with the onset of the experimental spectrum, unlike the predicted spectra obtained for conformers E–N. In particular, the spectrum of conformer D matches the experimental spectrum quite satisfactorily, reproducing all observed structures, though with different relative intensities. This particularly good agreement suggests that conformer D could be dominant in the experiment, at odds with harmonic calculations based on the wB97xD density functional. However, when the conformers are reoptimized using the DFT/M06-2X method with the aug-cc-pVTZ basis set instead, conformer D, the achiral conformer, is indeed found as the lowest in energy [see Fig. S5]. All data regarding the calculations at the DFT/M06-2X/aug-cc-pVTZ and DFT/wB97xD/6-311++G** level of theory including electronic and zero-point vibrational energies are provided in Table S2 and S3. However, no significant variations were found for the VIE and AIE of the most stable conformers calculated with the two DFT methods [see FIG. S6], nor the structures themselves, and the wB97xD/6-311++G** method was adopted for computations of clusters of hexene conformers.

### B. Clusters of 1-hexene

Using the methods described in Sec. 3, candidate structures for 1-hexene clusters ranging from dimers to octamers were predicted through the combination of systematic sampling of their energy landscapes assuming rigid conformers from the pool of 27 available structures and model pairwise interactions described with a force field, followed by DFT reoptimization at the wB97xD/6-311++G** level of theory. The resulting structures are depicted in FIG. 5, with one or two structures for each cluster size depending on even more stable structures being found upon inclusion of the zero-point harmonic vibrational correction.

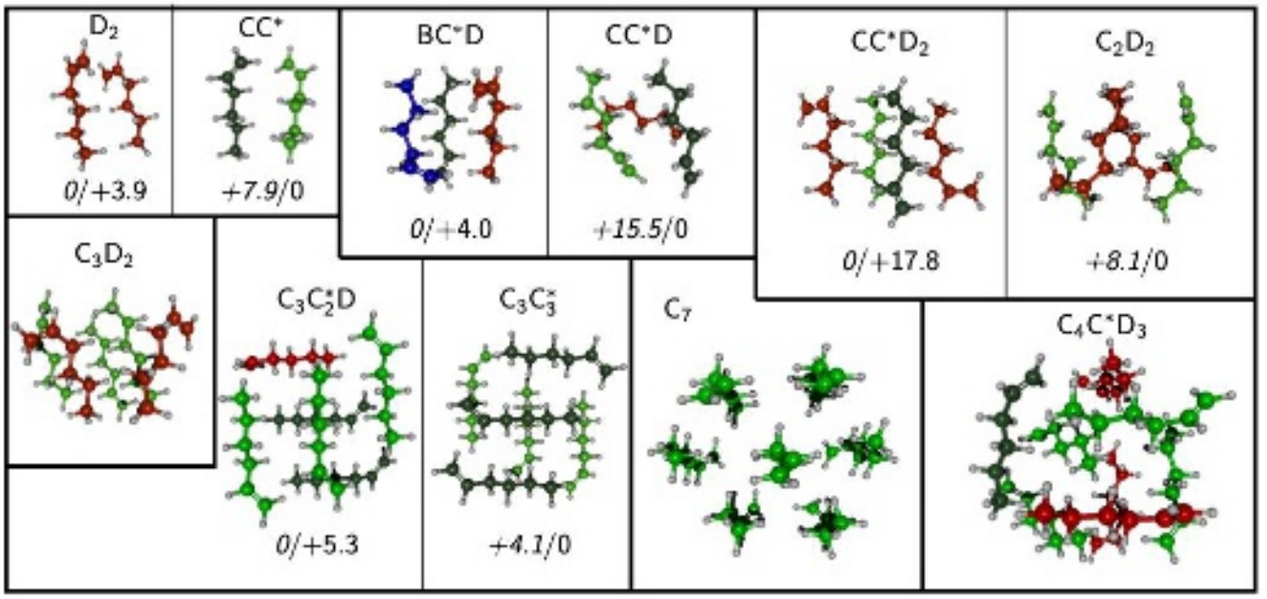


FIG. 5. Lowest-energy structural candidates predicted for 1-hexene clusters containing 2 to 8 molecules. Colors refer to specific monomer conformers A—D chosen to compose the clusters and identified as the most likely components of clusters. The asterisk in C* indicates the enantiomer of conformer C. For competing structures, the relative energies (meV) are provided *without*/with harmonic zero-point energy correction.

Overall, the stable structures show a rather high degree of alignment between hexene molecules, conformers C and D, in particular, appearing mostly elongated and prone to herringbone-like arrangements. Other conformers do not allow such alignment, with the exception of conformer B which is found to contribute to the lowest-energy classical structure of the trimer. Apart from the hexamer and the octamer, all clusters thus exhibit structures in which the carbon backbones are essentially parallel to one another, the monomers arranging themselves through interdigitation. In several cases, optimal interdigitation is achieved by combining different monomers, hence the frequent coexistence of conformers D, C, and its enantiomer C*. The most elaborate form with aligned elongated monomers is reached for the heptamer, in which the backbone axes are distributed on a triangular lattice [see FIG. 5, $C_7$ structure]. At this size, the cluster forms a nearly isotropic atomic arrangement, and the addition of an $8^{th}$ molecule breaks this high degree of ordering, leading to a somewhat disordered mixture of C, C*, and D conformers. An alternative arrangement is found specifically for the hexamer, whose two candidate structures are both composed of three parallel monomers rotated by 90° underneath the three other monomers, also parallel with each other.

Before discussing aspects related to electronic structure, it is important to emphasize here that the clusters themselves are expected to be rather fluxional under the experimental conditions close to 130 K. The canonical heat capacities obtained from the parallel tempering Monte Carlo simulations, a selection of which are provided as supplementary material [see FIG. S7], systematically show bumps at temperatures that are lower or close to this value that are the signature of isomerization and fluxionality. Marked differences are also found for a given cluster size (here BC*D versus CC*D), indicating also a strong sensitivity to the structural details. From the parallel tempering Monte Carlo simulations, periodic quenches were performed

to determine the distributions of local minima visited as a function of temperature. The distributions obtained near 130 K, illustrated in FIG. S8 for the specific clusters highlighted in FIG. 5 and containing up to 5 monomers, are always broad and extend over 100-300 meV above the putative global minimum, depending on cluster size. Interestingly, they are particularly broad and smooth for most systems, indicating liquid-like regimes, with the notable exception of $C_2D_2$ for which the distribution is narrower and dominated at this temperature by low-energy structures, although it still reflects the coexistence of more than a hundred independent local minima.

The picture emerging from these statistical distributions is that a strong coexistence between many isomers is to be expected under the experimental conditions. While conformers C and C*, D and, to a lesser extent, B and B* seem to dominate the distributions, the differences in energy between the various cluster structures are extremely small, and the absence of any narrow feature in the heat capacity curves suggests that no particular structure is stabilized by entropy.

This word of caution being kept in mind, and without direct experimental evidence for specific structures, the putative global minima identified in the previous step were used as the starting point of quantum chemistry calculations of their ionization energies. The quantum chemical methods employed to determine vertical and adiabatic ionization energies of the various conformers of the hexene monomer are too computationally expensive to be used in the entire size range extending to the octamer, but they are still applicable for selected structures up to the pentamer, DFT appearing as the only approach among our arsenal to cover the hexamer, heptamer, and octamer. TABLE I summarizes the results of these calculations, for the structures depicted in FIG. 3 as well as the most relevant conformers identified for the monomer, namely A and D.

TABLE I. Vertical (VIE) and adiabatic (AIE) ionization energies of 1-hexene clusters obtained from different quantum chemical methods as a function of the number of monomers

| Cluster | Type | Ionization energy (eV) | | | | | |
|---|---|---|---|---|---|---|---|
| | | *VIE* | AIE | AIE | | | |
| | | wB97xD[a] | | (R)CCSD(T)-F12[b] | CBS-QB3 | (R)MP2-F12[c] | (R)MP2[d] |
| 1 | A | *9.52* | 9.15 | 9.49 | 9.51 | 9.63 | 9.42 |
| | D | *9.55* | 9.17 | 9.55 | 9.54 | 9.61 | 9.40 |
| 2 | CC* | *9.65* | 8.22 | 8.54 | 8.49 | 8.34 | 8.16 |
| | D2 | *9.17* | 8.58 | 8.90 | 8.87 | 8.75 | 8.51 |
| 3 | BC*D | *9.18* | 8.48 | … | … | 8.65 | 8.44 |
| | CC*D | *8.99* | 8.12 | … | … | 8.25 | 8.05 |
| 4 | C2D2 | *9.16* | 9.12 | … | … | 9.23 | 9.00 |
| | CC*D2 | *9.15* | 9.05 | … | … | 9.14 | 8.91 |
| 5 | C3D2 | *9.09* | 8.74 | … | … | … | … |
| 6 | C3C3* | *8.93* | 8.18 | … | … | … | … |
| | C3C2*D | *8.94* | 8.19 | … | … | … | … |
| 7 | C7 | *8.89* | 8.07 | … | … | … | … |
| 8 | C4C*D3 | *8.92* | 8.23 | … | … | … | … |

[a]wB97xD/6-311++G**
[b](R)CCSD(T)-F12/aug-cc-pVDZ
[c](R)MP2-F12/aug-cc-pVDZ
[d](R)MP2/aug-cc-pVDZ

Overall, all methods concur in predicting a general decrease in the ionization energy with increasing cluster size, a feature previously observed for other hydrocarbon clusters made from polyaromatic units [76],[77] and found here to be more pronounced for vertical ionization energies. The decreasing trend is consistent with the expected increasing electron delocalization [78]. In general, the adiabatic ionization energies are ordered as (R)MP2-F12>wB97xD>(R)MP2. For the dimer, AIE values agree between the (R)CCSD(T)-F12 and CBS-QB3 methods. Unlike the monomer, for which this agreement was anticipated owing to (R)CCSD(T) data being a final component of CBS-QB3 calculations, here it could be more fortuitous because geometry optimization performed with the DFT/B3LYP method ignores non-covalent interactions that are expected to be essential for neutral clusters. We thus interpret the good performance of CBS-QB3 for hexene dimers as the manifestation of very minor rearrangements in the neutral structure with this hybrid functional. Interestingly, the smaller size variations exhibited by the AIE with the DFT method are concomitant with their greater sensitivity to structural details, as seen by the substantial dispersion of AIE values obtained individually for the 196 dimers and 85 trimers [see FIG. S9]. Such a sensitivity arises due to the diversity in the intermolecular arrangements of the neutral clusters seen in FIG. 2, which react very differently upon electron removal and produce chemically distinct cationic minima. In contrast, the much narrower distributions of VIE values obtained for the dimers and trimers, about 0.2 eV, is actually comparable in magnitude to the corresponding dispersion in the monomer [see FIG. 3], which indicates that intermolecular interactions have only a minor influence on the precise value of the VIE in clusters, except for overall size effects. Interestingly, a similar spreading of 0.2 eV is found for the binding energy among neutral clusters themselves. Fig. S10, S11, and S12 show the distributions of energies obtained at the DFT level for the 196 dimers, 85 trimers, and 109 tetramers considered, respectively, relative to the lowest values. The figures also highlight the possible change in ordering caused by including the harmonic zero-point energy.

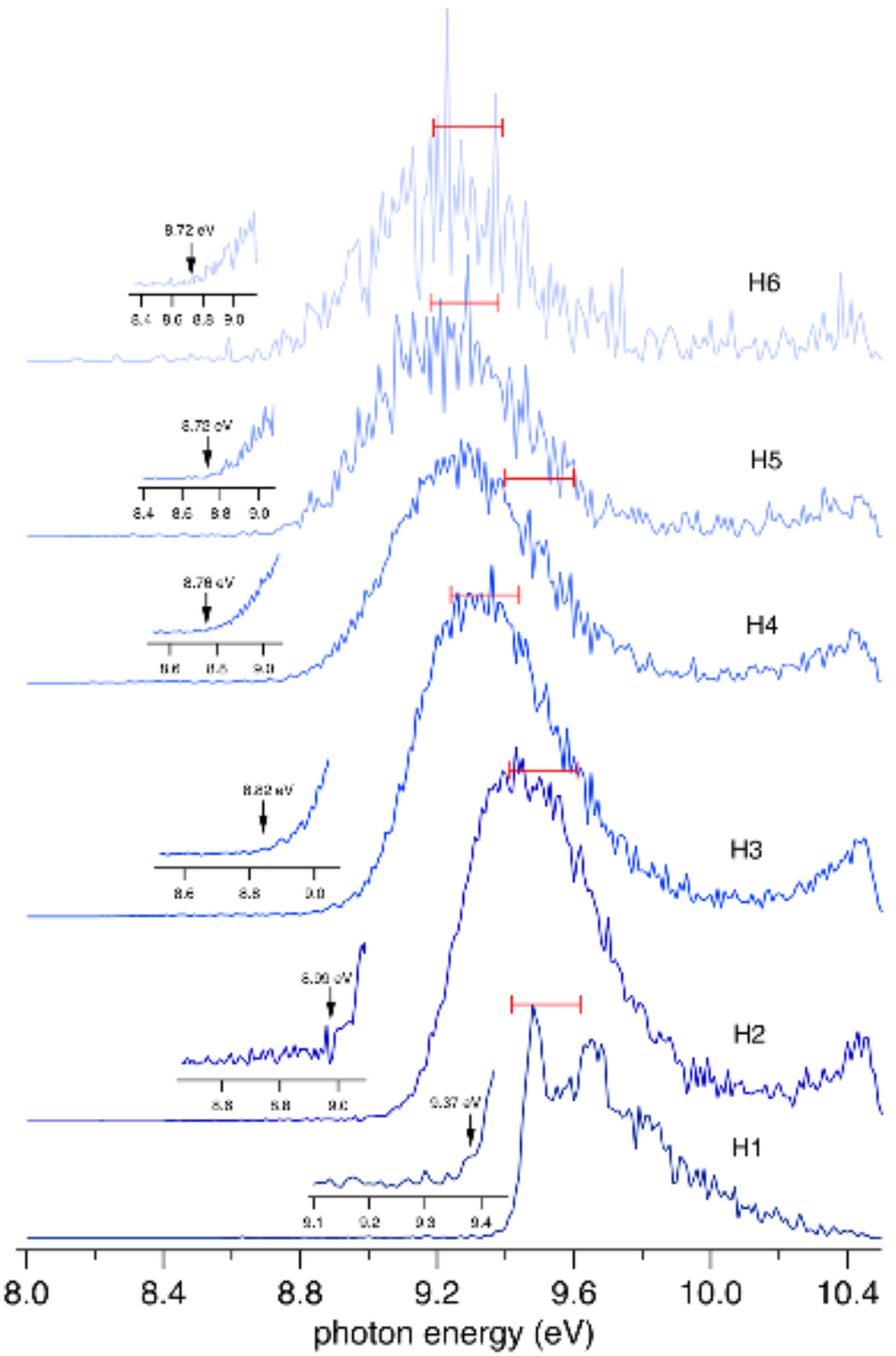


FIG. 6. Experimental threshold photoelectron spectra measured for 1-hexene (H*n*, *n* = 1–6) clusters, ranging from the monomer (H1) to the hexamer (H6). The arrows point to the estimated ionization threshold (see text for details), while the horizontal bars highlight the predicted VIE values obtained from DFT/wB97xD/6-311++G** calculations corrected by a constant shift to reproduce (R)CCSD(T)-F12 data (see text for details). An uncertainty of 0.1 eV was associated with the calculated values to account for possible intrinsic computational errors. The insets display magnified views of the low-energy portion of the TPES, providing a clearer distinction of the ionization threshold.

FIG. 6 shows the experimental TPES obtained for 1-hexene clusters up to the hexamer as well as the calculated VIE. By looking at the energy shift of the spectra, a comparable decreasing trend with increasing size is noticed as the calculated VIE

with the DFT method in the comparable size range, the main difference being a systematic shift of 0.3–0.4 eV. According to Table I, the energy difference between the AIEs of the dimer calculated using DFT and (R)CCSD(T)-F12 methods is similar to the difference found for the various conformers of the monomer (see FIG. S2) and approximately equal to 0.35 eV, a value precisely comparable to the aforementioned shift. Assuming now this difference to be intrinsic to the method rather than the details of the molecular system, it can be considered as fixed and can be used to recalibrate the DFT values towards (R)CCSD(T) accuracy. By applying this correction and adding a typical uncertainty of 0.1 eV to account for intrinsic inaccuracies in the underlying quantum chemical methodology, as well as the aforementioned thermal fluctuations caused by the likely fluxional character of such van der Waals clusters at 130 K, variations in ionization energy with increasing size are observed. These variations are represented in FIG. 7, where the ionization threshold inferred from the TPES in FIG. 6 is compared to the calculated AIE.

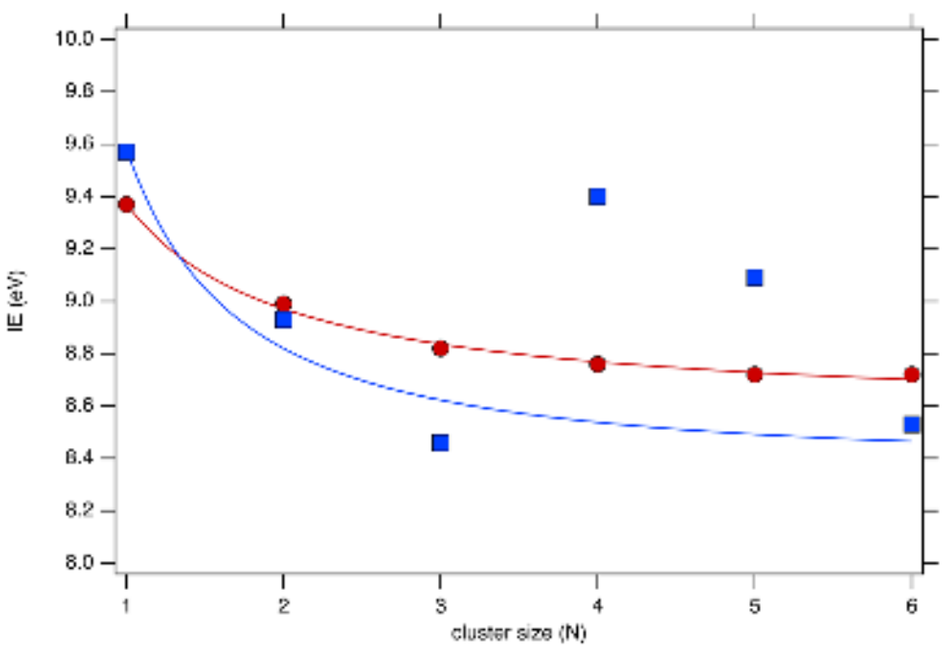


FIG. 7. Comparison between inferred ionization thresholds (red dots) and corrected theoretical AIEs from DFT for the 1-hexene monomer and clusters (blue squares). Colored lines refer to different fits using a power function (see text for details).

The TPES spectra of H2–H6 (FIG. 6) are characterized by a slow increase in signal that originates from the increasing structural flexibility of the molecular clusters due to unfavorable FC factors upon single photon ionization of the corresponding neutrals. This makes determining their AIEs very difficult, as it is far from the main vibronic transition. This difficulty is also reflected in the large deviations between the VIEs and AIEs [see TABLE I], which can exceed 1 eV in some cases. Consequently, the literature primarily relies on comparisons of VIEs [76],[79]. FIG. 7 presents the calculated AIEs alongside the inferred ionization thresholds derived from the TPES spectra in FIG. 6. Noticeably, these thresholds are not a direct

experimental determination of AIEs but were instead set at the lowest photon energy where the TPES signal exceeds the baseline noise level [77],[80]. FIG. 7 indicates a general linear decrease in these thresholds with increasing cluster size through the red line which corresponds to a fit of the data using a power function with the form $y_0 + An^B$, where $n$ is the variable related to the cluster size [81],[82]. For large clusters, the IE often exhibits an inverse linear relationship with the number of atoms or cluster radius, likely due to charge delocalization across extended systems [78]. This trend is similarly observed in the calculated AIEs with the blue line in FIG. 7, if the data for the tetramer and pentamer that slightly exceed the values for the adjacent clusters are ignored. Such deviations may arise from quantum size effects, electronic shell closures, or specific geometric structures [83]. However, from the calculated distributions of isomer spreading (FIG. S8, S10-S12), it is much more likely that the structures of these clusters at 130 K significantly deviate from the low-energy candidates selected for the electronic structure studies. The overall trend of decreasing IE with larger clusters corresponds to increased electron delocalization, which stabilizes the molecule and reduces the energy needed to remove an electron. The trimer and hexamer represented in FIG. 5 have relatively cohesive and extended structures, likely promoting greater delocalization. However, the tetramer and pentamer configurations can restrict delocalization due to localized high electron density areas or structural asymmetries with limited continuity, that can contribute to higher IEs. The issue of electron delocalization is further complicated by the possible delocalization of the cationic structures themselves. While most of the geometries considered in FIG. 5 produce optimized cations that are essentially similar to the neutral structures, up to some overall deformations, proton-shared cations are also occasionally found, as is the case here for the BC*D trimer, depicted in FIG. S13. Proton-shared oligomers are commonly featured in cationic molecular clusters [84], and arise here due to the proximity between the ethylene tail of one molecule and an hydrogen bonded to a sp3 carbon of another molecule. This electronic effect will in turn further contribute to the vibrational flexibility of the cationic clusters, making the static picture advocated here even more disputable.

Despite of the uncertainties clearly found in the structures selected for the tetramer and pentamer, the discrepancy in the ionization energies at these sizes is also evident in FIG. 6, where the calculated VIE exceeds the maximum TPES signal. Based on FIG. S8 and the significant spread exceeding 0.2 eV for the trimer, this discrepancy indicates that the specific structures considered here, based on combinations of C, C*, and D monomers, may not represent the free-energy minima effectively sampled at 130 K. Such minima could be in principle determined from our database of structures, but this would be computational excessively involved due to the need for performing not only geometry minimizations at the DFT level but, more importantly, vibrational analyses. Moreover, the significant broadening in the isomers' distributions at the experimental temperature, already for the monomer, shows that hexene clusters should be strongly fluxional under these conditions, hence matching the experimentally measured ionization energy to a value calculated for a specific isomer would likely be

inconclusive. Isomer fluxionality will also necessarily hamper any chiral recognition effect, which would otherwise be manifested by preferential oligomers involving specific sets or combinations of enantiomers.

## V. CONCLUSION

The structural and electronic properties of clusters of an archetypal olefin molecule, 1-hexene, were investigated experimentally using VUV PEPICO spectroscopy assisted with a multi-approach computational investigation of the low-energy structures and their vertical and adiabatic ionization energies. Both approaches concur in showing a clear size dependence of the ionization energies of these clusters, both adiabatic and vertical ionization energies decreasing with increasing cluster size. This trend is consistent with previous studies on PAH clusters [77], supporting the idea that as clusters grow, the energy required to ionize them decreases due to increased electron delocalization and stabilization. The theoretical support for this observation lies in the concept that larger clusters can distribute the electron density more evenly across their expanded structures, thereby reducing the energy barrier for ionization. This is further evidenced by the flexible nature of 1-hexene monomers, which can adopt multiple energetically similar conformations, most of them also having a chiral character that leads to a very broad variety of possible cluster geometries. As cluster size increases, the number of possible arrangements grows exponentially, and under the experimental temperature conditions our simulations further suggest a high degree of fluxionality, all factors combined contributing to a broad range of potential ionization energies.

Admittedly, our theoretical work also faced significant difficulties in evaluating ionization energies for clusters larger than the tetramer (72 atoms), the most accurate wavefunction-based methods becoming computationally demanding and necessarily limited to few candidate structures. While the results presently obtained for the tetramer clusters deviate the most significantly from the experimental trends otherwise well reproduced, they still fall within 0.3 eV from the measured ionization threshold value, a discrepancy that could be evaluated to be close to the intrinsic variations due to temperature effects for these clusters under the present experimental conditions. To assess whether isomer fluxionality is the cause of the discrepancy for the tetramer and the pentamer, a more thorough for the lowest free-energy structures should be conducted. A statistical survey of the possible preference for specific enantiomers and their joint occurrence could also be useful to get further insight into chiral recognition effects and their temperature dependence.

## SUPPLEMENTARY MATERIAL

Supplementary material provides detailed geometries of the different conformers of the monomer, needed to build the initial structures of the clusters along with additional Franck-Condon factors and ionization energy. Canonical heat capacities of selected clusters and distribution of the ionization energy for the dimer and trimer are also provided.

## ACKNOWLEDGMENTS

We acknowledge SOLEIL for provision of synchrotron radiation under project 20210964 and we are grateful to J.-F. Gil for his technical help around the SAPHIRS set-up. We thank the QUADMARTS International Research Network for promoting the collaboration. This work was performed using HPC resources from the EXPLOR center hosted by the University of Lorraine (Project: 2021EXTXX2356). The authors extend their appreciation to the Researchers Supporting Project (RSPD2025R808) of King Saud University, Riyadh, Saudi Arabia.

## AUTHOR CONTRIBUTIONS

CSL, OH, PA, LST, GV, FBL, and JB collected the experimental data. GAG, MAM and LN provided support for the analysis. MH, FC, and JB performed the theoretical calculations, analyzed the data and wrote the original draft. All the authors contributed to review the final manuscript.

## REFERENCES

[1] H.J. Zeng, N. Yang, and M.A. Johnson, Faraday Discuss. 217, 8 (2019).
[2] M. Fárník and J. Lengyel, Mass Spectrom. Rev. 37, 630 (2018).
[3] V. Vaida, J. Chem. Phys. 135, (2011).
[4] O. Dopfer and M. Fujii, Chem. Rev. 116, 5432 (2016).
[5] H. Schwarz, Catal. Sci. Technol. 7, 4302 (2017).
[6] M. Juanes, R.T. Saragi, W. Caminati, and A. Lesarri, Chemistry A European J 25, 11402 (2019).
[7] E. Jimenez-Izal and A.N. Alexandrova, Annu. Rev. Phys. Chem. 69, 377 (2018).
[8] J. Yao, D.B. Lao, X. Sui, Y. Zhou, S.K. Nune, X. Ma, T.P. Troy, M. Ahmed, Z. Zhu, and D.J. Heldebrant, Phys. Chem. Chem. Phys. 19, 22627 (2017).
[9] G.-L. Hou, W. Lin, and X.-B. Wang, Commu. Chem. 1, 37 (2018).
[10] L. Ban, B.L. Yoder, and R. Signorell, Annu. Rev. Phys. Chem. 71, 315 (2020).
[11] R. Signorell and B. Winter, Phys. Chem. Chem. Phys. 24, 13438 (2022).
[12] A.S. Zaag, O. Yazidi, N.-E. Jaidane, M.W. Ross, A.W.Jr. Castleman, M.M. Al Mogren, R. Linguerri, and M. Hochlaf, J. Phys. Chem. A 120, 1669 (2016).
[13] F. Calvo, Phys. Rev. E 60, 2771 (1999).
[14] E. Sennert and M.A. Suhm, Phys. Chem. Chem. Phys. (2024).
[15] V. Strelkov, U. Saalmann, A. Becker, and J.M. Rost, Phys. Rev. Lett. 107, 113901 (2011).
[16] T.E. Gartmann, S. Hartweg, L. Ban, E. Chasovskikh, B.L. Yoder, and R. Signorell, Phys. Chem. Chem. Phys. 20, 16364 (2018).
[17] R. Signorell, B.L. Yoder, A.H. West, J.J. Ferreiro, and C.-M. Saak, Chem. Sci. 5, 1283 (2014).
[18] D. Rolles, H. Zhang, Z.D. Pešić, R.C. Bilodeau, A. Wills, E. Kukk, B.S. Rude, G.D. Ackerman, J.D. Bozek, R. Díez Muiño, F.J. García De Abajo, and N. Berrah, Phys. Rev. A 75, 031201 (2007).
[19] M. Ahmed and O. Kostko, Phys. Chem. Chem. Phys. 22, 2713 (2020).
[20] I. Fischer and S.T. Pratt, Phys. Chem. Chem. Phys. 24, 1944 (2022).
[21] T. Baer and R. P. Tuckett, Phys. Chem. Chem. Phys. 19, 9698 (2017).
[22] H. Shiromaru and S. Katsumata, Bull. Chem. Soc. Jpn. 57, 3543 (1984).
[23] J. Hernández-Rojas, F. Calvo, S. Niblett, and D.J. Wales, Phys. Chem. Chem. Phys. 19, 1884 (2017).

[24] M. Hochlaf, Phys. Chem. Chem. Phys. 19, 21236 (2017).
[25] G.A. Garcia, L. Dontot, M. Rapacioli, F. Spiegelman, P. Bréchignac, L. Nahon, and C. Joblin, Phys. Chem. Chem. Phys. 25, 4501 (2023).
[26] S. Hartweg, G.A. Garcia, and L. Nahon, J. Phys. Chem. A 125, 4882 (2021).
[27] S. Hartweg, B.L. Yoder, G.A. Garcia, L. Nahon, and R. Signorell, Phys. Rev. Lett. 118, 103402 (2017).
[28] T.S. Totton, A.J. Misquitta, and M. Kraft, Physical Chemistry Chemical Physics 14, 4081 (2012).
[29] C. Shao, Q. Wang, W. Zhang, A. Bennett, Y. Li, J. Guo, H.G. Im, W.L. Roberts, A. Violi, and S.M. Sarathy, Commun. Chem. 6, 223 (2023).
[30] H. Wang, Proc. Combust. Inst. 33, 41 (2011).
[31] K.O. Johansson, M.P. Head-Gordon, P.E. Schrader, K.R. Wilson, and H.A. Michelsen, Science 361, 997 (2018).
[32] B.A. Adamson, S.A. Skeen, M. Ahmed, and N. Hansen, Z. Phys. Chem. 234, 1295 (2020).
[33] I.J. Webster, J.L. Beckham, N.D. Johnson, and M.A. Duncan, J. Phys. Chem. A 126, 1144 (2022).
[34] M.R. Kholghy, G.A. Kelesidis, and S.E. Pratsinis, Phys. Chem. Chem. Phys. 20, 10926 (2018).
[35] X. Mercier, O. Carrivain, C. Irimiea, A. Faccinetto, and E. Therssen, Phys. Chem. Chem. Phys. 21, 8282 (2019).
[36] A. Faccinetto, C. Irimiea, P. Minutolo, M. Commodo, A. D'Anna, N. Nuns, Y. Carpentier, C. Pirim, P. Desgroux, C. Focsa, and X. Mercier, Commun. Chem. 3, 112 (2020).
[37] H. Sabbah, L. Biennier, S.J. Klippenstein, I.R. Sims, and B.R. Rowe, J. Phys. Chem. Lett. 1, 2962 (2010).
[38] A. Tielens, in *Dust and Chemistry in Astronomy* (Routledge, 2019), pp. 103–141.
[39] C. Joblin and A.G.G.M. Tielens, in *PAHs and the Universe* (EDP sciences, 2021).
[40] J.E. Roser and A. Ricca, Proc Int Astron Union 15, 415 (2019).
[41] J.E. Roser and A. Ricca, Astrophys. J. 801, 108 (2015).
[42] L.J. Allamandola, A. Tielens, and J.R. Barker, Astrophys. J. Suppl. Ser. (ISSN 0067-0049), Vol. 71, Dec. 1989, p. 733-775. Research Supported by NASA, DOE, and NSF. 71, 733 (1989).
[43] L.S. Bernstein and T.R. Geballe, Astrophys. J. 962, 114 (2024).
[44] M. Rapacioli, F. Calvo, C. Joblin, P. Parneix, D. Toublanc, and F. Spiegelman, Astron. Astrophys. 460, 519 (2006).
[45] Y. Yang, C. Zhang, X. Hu, D. Zhang, Y. Chen, J. Zhen, and L. Qin, Mon. Not. R. Astron. Soc. 508, 3009 (2021).
[46] J. Zhen, T. Chen, and A.G. Tielens, Astrophys. J. 863, 128 (2018).
[47] J. Zhen, Y. Yang, W. Zhang, and Q. Zhu, Astron. Astrophys. 628, A57 (2019).
[48] J.B.P. Soares and T.F.L. McKenna, *Polyolefin Reaction Engineering*, Weinheim, Germany: Wiley-VCH (2012).
[49] J. Bourgalais, Z. Jiang, J. Bloino, O. Herbinet, H.-H. Carstensen, G.A. Garcia, P. Arnoux, L.-S. Tran, G. Vanhove, L. Nahon, F. Battin-Leclerc, and M. Hochlaf, Phys. Chem. Chem. Phys. 24, 10826 (2022).
[50] L. Nahon, N. de Oliveira, G.A. Garcia, J.-F. Gil, B. Pilette, O. Marcouillé, B. Lagarde, and F. Polack, J. Synchrotron Radiat. 19, 508 (2012).
[51] G.A. Garcia, B.K. Cunha de Miranda, M. Tia, S. Daly, and L. Nahon, Rev. Sci. Instrum. 84, 053112 (2013).
[52] X. Tang, G.A. Garcia, J.-F. Gil, and L. Nahon, Rev. Sci. Instrum. 86, 123108 (2015).
[53] G.A. Garcia, L. Nahon, and I. Powis, Rev. Sci. Instrum. 75, 4989 (2004).
[54] J.C. Poully, J.P. Schermann, N. Nieuwjaer, F. Lecomte, G. Grégoire, C. Desfrançois, G.A. Garcia, L. Nahon, D. Nandi, L. Poisson, and M. Hochlaf, Phys. Chem. Chem. Phys. 12, 3566 (2010).
[55] M. Briant, L. Poisson, M. Hochlaf, P. de Pujo, M.-A. Gaveau, and B. Soep, Phys. Rev. Lett. 109, 193401 (2012).
[56] A. Candian, J. Bouwman, P. Hemberger, A. Bodi, and A.G. Tielens, Phys. Chem. Chem. Phys. 20,

5399 (2018).
[57] S. Morgan and A.W. Castleman, J. Phys. Chem. 93, 4544 (1989).
[58] O. Echt, P.D. Dao, S. Morgan, and A.W. Castleman Jr, J. Chem. Phys. 82, 4076 (1985).
[59] L. Dontot, F. Spiegelman, and M. Rapacioli, J. Phys. Chem. A 123, 9531 (2019).
[60] J.-D. Chai and M. Head-Gordon, Phys. Chem. Chem. Phys. 10, 6615 (2008).
[61] M. Petković, J. Phys. Chem. A 116, 364 (2012).
[62] J. Wang, P. Cieplak, and P.A. Kollman, J. Comput. Chem. 21, 1049 (2000).
[63] J. Zeng, L. Duan, J.Z.H. Zhang, and Y. Mei, J. Comput. Chem. 34, 847 (2013).
[64] Y. Majdi, M. Hochlaf, Y. Pan, K.-C. Lau, L. Poisson, G.A. Garcia, L. Nahon, M.M. Al-Mogren, and M. Schwell, J. Phys. Chem. A 119, 5951 (2015).
[65] K. Laamiri, G.A. Garcia, L. Nahon, A. Ben Houria, R. Feifel, and M. Hochlaf, Phys. Chem. Chem. Phys. 24, 3523 (2022).
[66] Y. Pan, K.-C. Lau, L. Poisson, G.A. Garcia, L. Nahon, and M. Hochlaf, J. Phys. Chem. A 117, 8095 (2013).
[67] H. Yan Zhao, K.-C. Lau, G. A. Garcia, L. Nahon, S. Carniato, L. Poisson, M. Schwell, M. Mogren Al-Mogren, and M. Hochlaf, Phys. Chem. Chem. Phys. 20, 20756 (2018).
[68] H.-J. Werner, P.J. Knowles, G. Knizia, F.R. Manby, and M. Schütz, WIREs Comput. Mol. Sci. 2, 242 (2012).
[69] T.H. Dunning, J. Chem. Phys. 90, 1007 (1989).
[70] R.A. Kendall, T.H. Dunning, and R.J. Harrison, J. Chem. Phys. 96, 6796 (1992).
[71] J. Bourgalais, X. Mercier, M.M. Al-Mogren, and M. Hochlaf, J. Phys. Chem. A 127, 8447 (2023).
[72] J.A. Montgomery, M.J. Frisch, J.W. Ochterski, and G.A. Petersson, J. Chem. Phys. 110, 2822 (1999).
[73] J.A. Montgomery, M.J. Frisch, J.W. Ochterski, and G.A. Petersson, J. Chem. Phys. 112, 6532 (2000).
[74] J. Bloino, A. Baiardi, and M. Biczysko, Int. J. Quantum Chem. 116, 1543 (2016).
[75] J. Bourgalais, C. Smith Lewin, O. Herbinet, G.A. Garcia, P. Arnoux, L.-S. Tran, G. Vanhove, L. Nahon, and F. Battin-Leclerc, Combust. Flame 258, 113065 (2023).
[76] S.R. Domingos, D.S. Tikhonov, A.L. Steber, P. Eschenbach, S. Gruet, H.R. Hrodmarsson, K. Martin, G.A. Garcia, L. Nahon, and J. Neugebauer, Nat. Commun. 15, 4928 (2024).
[77] C. Joblin, L. Dontot, G.A. Garcia, F. Spiegelman, M. Rapacioli, L. Nahon, P. Parneix, T. Pino, and P. Bréchignac, J. Phys. Chem. Lett. 8, 3697 (2017).
[78] S. Barth, M. Ončák, V. Ulrich, M. Mucke, T. Lischke, P. Slavíček, and U. Hergenhahn, J. Phys. Chem. A 113, 13519 (2009).
[79] Y.L. Chen, C.A. Taatjes, and G. Meloni, ChemPhysChem 25, e202300896 (2024).
[80] I. Derbali, H.R. Hrodmarsson, Z. Gouid, M. Schwell, M.-C. Gazeau, J.-C. Guillemin, M. Hochlaf, M.E. Alikhani, and E.-L. Zins, Phys. Chem. Chem. Phys. 21, 14053 (2019).
[81] S.H. Linn, Y. Ono, and C.Y. Ng, J. Chem. Phys. 74, 3342 (1981).
[82] W.M. Trott, N.C. Blais, and E.A. Walters, J. Chem. Phys. 69, 3150 (1978).
[83] L. Belau, S.E. Wheeler, B.W. Ticknor, M. Ahmed, S.R. Leone, W.D. Allen, H.F. Schaefer, and M.A. Duncan, J. Am. Chem. Soc. 129, 10229 (2007).
[84] S. Hartweg, M. Hochlaf, G.A. Garcia, and L. Nahon, J. Phys. Chem. Lett. 14, 3698 (2023).